Time scales of the Bipolar seesaw: The role of oceanic cross-hemisphere signals, Southern Ocean eddies and wind changes

Laurits S. Andreasen

Handed in: November 29, 2019

Advisor: Markus Jochum

Abstract

The coupling between Dansgaard-Oescher events and Antarctic Isotope Maximas, together known as the bipolar seesaw, is a prominent example of interhemispheric teleconnection in the earth system. The bipolar seesaw has been reproduced in coupled earth system models, but it is still not clear which physical mechanisms facilitate this. The coupled models find changes in both ocean thermal structure and the atmospheric circulation, and their interdependence is not clear. To gain insight in this interdependence, we perturb an ocean general circulation model with a combination of salinity perturbations and changes in atmospheric forcing. These forcing changes are inspired by changes found in the atmosphere in coupled models, that simulates the bipolar seesaw. We find that the response time of the ocean thermocline to the salinity perturbations is insensitive to the changes in atmospheric forcing. We also find that the response time is insensitive to whether the salinity perturbation is fresh or salt, and to the magnitude of the eddy diffusion constant. A short integration of a high resolution setup and a scale analysis indicate time scales in the same range as the coarse resolution runs. This time scale - common for all diffusivites, the high resolution run and the scale analysis - is an order of magnitude smaller then ice core data suggest. From this mismatch it is suggested that changes in sea ice distributions and not oceanic adjustments are of major importance for the time scales revealed by ice cores.

Acknowledgements

Contents

1 Introduction - the bipolar seesaw[1]
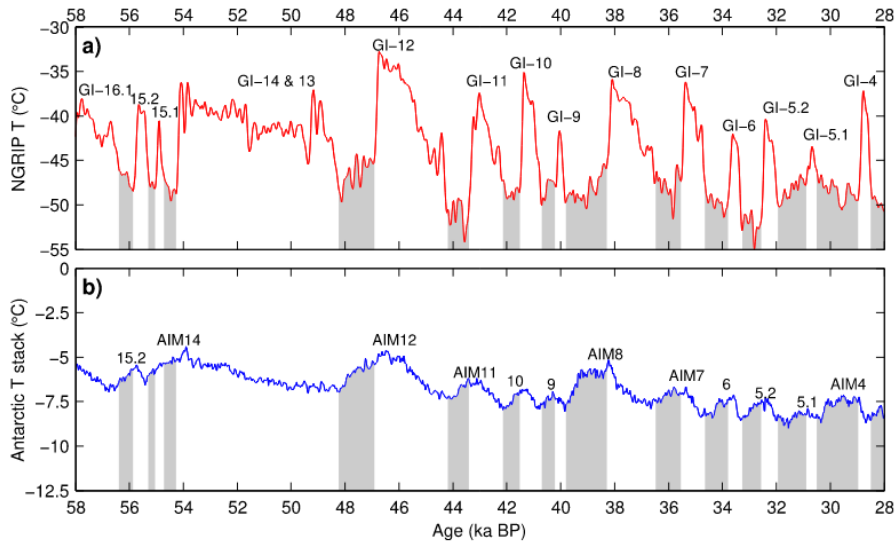
Figure 1.1: *The covariation of the Greenland and Antarctic temperature doing the last glacial. The GI-labels mark the beginning of a a Greenland interstadial, and AIM marks an Antarctic isotope maxima. The grey shading marks Greenland stadials. Adopted from Pedro et al. (2018).*

The climates of the two hemispheres of Earth are connected. A prominent example of this is known from the comparison of Greenland and Antarctic ice cores (Stocker and Johnsen (2003)). Here we see that during the last glacial sudden rises in Greenland temperature, the so called Dansgaard-Oescher events (DO), are followed by a delayed (∼200 years, WAIS Divide Project Members (2015), Buizert et al. (2018)) and more gradual fall in Antarctic temperature, the so called Antarctic Isoptope Maxima (AIM). This overall covariation is known as the bipolar seesaw.

The explanation of the seesaw pattern by Stocker and Johnsen (2003) is that the Southern Ocean (SO) acts as a heat reservoir, that keeps heat when Greenland is cold and releases it when Greenland warms up. In Pedro et al. (2018), a coupled earth system model is used to analyze the responses to fresh and salt water perturbations in the North Atlantic. These perturbations are suspected to have the same consequences as whatever mechanism triggers the stadial-interstadial transitions. The findings of Pedro et al. (2018) suggest that the seesawing is between the North Atlantic and the rest of the worlds oceans, and not between the SO and the rest of the oceans. Similar to the observed bipolar seesaw Pedro et al. (2018) finds that a fresh water perturbation in the North Atlantic leads to a delayed

---

[1]Parts of the work in this thesis has been submitted as *"Oceanic signal propagation from northern to southern high latitiudes in the Versatile Ocean Simulator"* to Ocean Modelling. The manuscript can be found in appendix B

increase in Antarctic temperature. Some notable adjustment effects of the fresh water perturbation of Pedro et al. (2018) where a weakening of equatorial winds, a southward shift of the westerlies over the SO, a deepening of the thermocline and melting of sea ice in the SO.

The oceanic adjustments to the fresh water perturbation travels as a warm heat anomaly through the Atlantic basin into the SO. It is not clear if the propagation of this signal is dependent on the atmospheric responses noted by Pedro et al. (2018) - that was a weakening of equatorial winds and a southward shift of the westerlies over the SO. To put constrains in this interdependence, we will investigate if the time it takes the ocean signal to travel from high northern latitude to high southern latitude is altered by the atmospheric changes.

Inviscid theories of the equatorial circulation suggest, that the equatorial circulation is rather insensitive to wind changes at the equator (Pedlosky (1991), Pedlosky (1987)). So the changes in the equatorial winds noted by Pedro et al. (2018) could happen without effect on the ocean circulation. As argued by Kawase (1987), changes in ocean density in one hemisphere can be communicated along the equator and lateral boundaries by Kelvin waves to the other hemisphere. Furthermore, changes can effect the interior of a basin through westward Rossby waves emitted from the Kelvin waves. It should be said, that the waves propagting at the western and eastern boundaries might be different from classical Kelvin waves, and have a slower Rossby-like character (Marshall and Johnson (2013)). Kawase (1987) therefore doesn't tell us how changes are communicated in the SO.

This was mentioned by Schmittner et al. (2003), who suggest that baroclinic eddies in the SO must play a key role in the heat transport. Some effects of baroclinic eddies on the mean flow are to flatten isopycnals and to transport tracers along isopycnals (Kuhlbrodt et al. (2012)). Both are very important processes for closing the overturning circulation (Kuhlbrodt et al. (2007)). The baroclinic eddies are often not resolved in ocean models, and are instead parameterized by the Gent-McWilliams (GM) parametrization (Gent et al. (1995); Gent and Mcwilliams (1990)). This parametrization will be explained in chapter 2, but the short version is, that the GM-parameterization induces a diffusion of isopycnal slopes, which corresponds to removal of potential energy (Griffies (1998); Vallis (2017)), and it induces diffusion of tracer quanteties along isopycnals (Redi (1982)). In the GM-parametrization a diffusion constant, κ, has to be chosen. Both a constant κ, and ones that vary in time and space are used in modelling (Eden et al. (2009)). Estimates of κ often ranges from 300 m^2s^{-1} to 2000 m^2s^{-1} (Kuhlbrodt et al. (2012)).

Though the perfect prescription of κ might be impossible to find, the parameterization is seen to reproduce similar tracer distributions to that of eddy resolving models (Poulsen et al. (2018)).

To deal with the uncertainty in the value of κ we will perform the same experiments

with different values of κ within the range of common values of climate models found by Kuhlbrodt et al. (2012). It should be said, that both observational evidence (Marshall et al. (2006)) and theoretical work (Ferrari and Nikurashin (2010)) suggest that low values ($< 500\text{m}^2\text{s}^{-1}$) can be found around jet cores in the SO. To address these potentially very low κ-values, an integration of an eddy resolving simulation will be done. An eddy resolving simulation doesn't rely on GM as much as a coarse resolution simulation. This could also make the flow less parabolic, which again could impact signal propagation.

The overall theme of this thesis will be interhemispheric teleconnection. We will perform an experiment similar to that of Pedro et al. (2018), where fresh and salt water is added in our model equivalent of the North Atlantic, and the questions we will address by this experiment, all inspired by Pedro et al. (2018), are:

1. Pedro et al. (2018) find that the salinity perturbation in the North Atlantic induces both changes in the atmospheric circulation and heat content of the ocean. The change in the oceanic heat content might be due to *direct adjustment* to the salinity perturbation. It might also have an *indirect contribution* from oceanic response to the wind changes. How do the *direct* and *indirect contribution* compare?

2. Pedro et al. (2018) finds that the zonal wind over the equator decreases in strength. How does it effect the travel time of the signal from the fresh water perturbation?

3. The winds over the ACC move slightly south in Pedro et al. (2018)'s study. How does this effect the travel time of the signal from the fresh water perturbation?

4. How does the travel time of signal depend on κ?

5. Is the response symmetric to the sign of the salinity perturbations?

6. Does the travel time change with improved resolution?

By answering these questions we hope to be able to determine if the adjustment time of the ocean to the salinity perturbation is sensitive to the changes in the atmospheric circulation and to κ. This will hopefully make it easier to constrain which processes are responsible for the progress of the temperature signal of Pedro et al. (2018).

2 Large scale eddy parameterization

The evolution of a tracer distribution in the ocean can be described by

$$\frac{\partial \phi}{\partial t} = \mathbf{u} \cdot \nabla \phi + D(\phi) + S, \tag{2.1}$$

Here t denotes time, $\mathbf{u}$ is the flow velocity found from the momentum and continuity equation, ϕ is the tracer concentration, and S contains sources and sinks. The term $D(\phi)$ can be understood in different ways depending on the interpretation of the tracer equation. One could interpret 2.1 as exact, and $D(\phi)$ would represent processes such as molecular diffusion, and we would have the classic advection-diffusion equation. One could also interpret 2.1 as some kind of average over e.g. a grid cell, ensemble members or a latitude line, then $D(\phi)$ will represent sub-grid scale processes and has to include the divergence of the product of deviations from the mean (Griffies (2003)):

$$D(\phi) = \nabla \cdot (\mathbf{u}'\phi') + ..., \tag{2.2}$$

where the stress mark indicates a deviations from a mean quantity.

Since most ocean models have to coarse a resolution to explicitly represent baroclinic mesoscale eddies, the term $\nabla \cdot (\mathbf{u}'\phi')$ must include the effect of these subgrid scale eddies on the grid scale tracer distribution. Since we don't know the value of the term, we will have to parametrize it. In the following we will present some classic closures for the term $\nabla \cdot (\mathbf{u}'\phi')$. In turbulence modelling the term "closure" means to express unresolved processes in terms of known mean variables.

2.1 Eddy diffusion along isopycnals

Our first assumption is that the unresolved eddies diffuses tracers a long isopycnals (Redi (1982); Kuhlbrodt et al. (2007)):

$$D(\phi) = \kappa_{iso}\nabla^2_\rho \phi + ... \tag{2.3}$$

Here ∇^2_ρ is the gradient along an isopycnal. The value of κ_{iso} can be both constant and varying in time and space (Eden et al. (2009)). This parameter influences how efficient eg. cold, fresh water is mixed with warm, salty water of the same density. Tæherefore the value og κ will have consequences for the time scales characterising transport of e.g. heat in the ocean.

2.2 Eddy diffusion of isopycnal steepness

Reducing the steepness of isopycnals is thought to be one of the major impacts baroclinic eddies have on the mean flow (Gent and Mcwilliams (1990)). As described in Vallis (2017), chapter 13, we can also think of this as diffusion of isopycnal steepness. Isopycnal steepness, $\mathbf{s}$, is defined by

$$\mathbf{s} = -\frac{\nabla_z \rho}{\frac{\partial \rho}{\partial z}}. \tag{2.4}$$

Here ρ is density, z is the vertical coordinate and ∇_z is the horizontal (constant z) gradient.

Another interpretation is that of Gent et al. (1995) who show that this will be the same as adding an extra advection term in the tracer equations calculated from the steepness of isopycnals.

$$D(\phi) = \tilde{\mathbf{u}} \cdot \nabla \phi + ... \tag{2.5}$$

Here $\tilde{\mathbf{u}} = (\tilde{\mathbf{v}}, \tilde{w})$ is the so-called bolus velocity given by

$$\tilde{\mathbf{v}} = -\frac{\partial}{\partial z}(\kappa_{GM}\mathbf{s}) \tag{2.6}$$

$$\tilde{w} = -\nabla_z(\kappa_{GM}\mathbf{s}) \tag{2.7}$$

The bolus velocity, $\tilde{\mathbf{u}}$ can be calculated from a common streamfunction, $\tilde{\psi} = \hat{\mathbf{k}} \times \kappa_{GM}\mathbf{s}$, with $\hat{\mathbf{k}}$ being the vertical unit vector. From 2.7 and 2.6 one could think, that increasing κ means increasing transport, but as argued below, this might not be the case.

It is numerically efficient and theoretically appealing to assume that $\kappa_{iso} = \kappa_{GM} = \kappa$ (Griffies (1998)). This will be done throughout this thesis.

When this assumption is satisfied, advection by the bolus velocity combined with along isopycnal diffusion, is equivalent to (Griffies (2003))

$$D(\phi) = \kappa \nabla \cdot \left(\nabla_z \phi - \mathbf{s}^2 \frac{\partial}{\partial z}\phi \right), \tag{2.8}$$

if the isolines of the tracer is parallel to isopycnals. This clearly illustrates, that the transport depends and both κ and $\mathbf{s}$.

2.3 Time scales of eddy diffusion

Nikurashin and Vallis (2011) argues that since in a zonal channel (as the southern part of Fig. 3.1) eddy fluxes and wind stress are nearly in balance, we have that $\kappa s \sim \tau/f_0$, where

s is the magnitude of $\mathbf{s}$, τ is the wind stress, and f_0 is the corriolis parameter. Assuming equality in this relation we get from eq. 2.8

$$D(\phi) = \nabla \cdot \left(\kappa \nabla_z \phi - \frac{\tau^2}{\kappa f_0^2} \frac{\partial}{\partial z} \phi \right),$$

(2.9)

With this the vertical transport of ϕ might even partially decrease with increasing κ. The diffusive flux can hence be decomposed into two parts, a horizontal and a vertical, with different effective diffusion strength. $k_y = \kappa$ in the horizontal, and $k_z = \tau^2/(\kappa f_0^2)$ in the vertical. For each direction a characteristic time scale can be associated (Landau and Lifshitz (1966)): $T_y = L_y^2/k_y = L_y^2/\kappa$ and $T_z = L_z^2/k_z = \kappa L_z^2 f_0^2/\tau^2$, where L_y are the characteristic length scale in the horizontal and L_z in the vertical. The horizontal transport therefore speeds up, when κ grows, whereas the vertical slows down.

To see how that influences the characteristic time of the combined vertical and horizontal process, we choose $L_z = 1\,\mathrm{km}$ - the scale of the channel depth, $L_y = 1000\,\mathrm{km}$ - the scale of the channel width, $f_0 = 10^{-4}\mathrm{s}^{-1}$, $\kappa = 1000\,\mathrm{m}^2\,\mathrm{s}^{-1}$ and $\tau = 10^{-4}\,\mathrm{N\,m\,kg}^{-1}$, we get $T_y \sim T_z \sim 10^9\,\mathrm{s} \sim 10$ years. This indicates that changing κ might have a rather small effect on the tracer change time scales, since the component of the time scale that grows with κ and the component that shrinks with κ are of similar magnitude.

The same conclusion can made from the derivative of the sum[1] of τ_y and τ_z with respect to κ:

$$\frac{\partial}{\partial \kappa}(\tau_y + \tau_z)\big|_{\kappa=1000\,\mathrm{m}^2\,\mathrm{s}^{-1}} = -\frac{L_y^2}{\kappa^2} + \frac{L_x^2 f_0^2}{\tau^2}\big|_{\kappa=1000\,\mathrm{m}^2\,\mathrm{s}^{-1}} = 0$$

(2.10)

So as long as $\kappa \sim 1000\,\mathrm{m}^2\,\mathrm{s}^{-1}$, the total time scale is constant in the first order to changes in κ.

The reason we choose L_y to be the width of the channel and not the length of the basin is, that wave processes with other time scales are thought to be dominant in the basin.

2.4 Other mixing processes

Not all mixing occurs along isopycnals. Breaking of internal waves and movements induced by small eddies (which might not be different things) can induce mixing across isopycnals. So-called diapycnal mixing. This mixing is important for establishing the mixed layer above the thermocline, and hence important for the upper winddriven part of the ocean circulation.

---

[1]How to combine the two timescales has not obvious. The reasoning behind the simple sum used here is that eq. 2.1 combined with eq. 2.9 and neglecting advection and the source term, do allow for a solution separated in vertical and horizontal coordinates. With the right initial and boundary condition a solution of the (Gaussian) form $\sim \exp\left(\tau_z(z-z_0)^2/t\right)\exp\left(\tau_y(y-y_0)^2/t\right) = \exp\left((\tau_z+\tau_y)/t\right)\exp\left((z-z_0)^2+(y-y_0)^2\right)$ is possible (Landau and Lifshitz (1966)). Here the two timescales appear combined as a sum.

2.5 Advection and diffusion dominated flows

With the assumptions about $D(\phi)$ from eq. 2.8, the partial differential equation 2.1 has both parabolic and hyperbolic characters. Hyperbolic systems (wave-like systems) are characterized by a finite propagation speed for disturbances, whereas parabolic systems (diffusion-like systems) have infinite propagation speed (Landau and Lifshitz (1966)). Note that the propagation speed is not the same as the characteristic time addressed in section 2.3, since that time scale tells how fast a system dominated by diffusion is saturated in a new steady state. Infinite propagation speed is of cause un-physical, but diffusion is easy to work with, and therefore often used as turbulence closures. The term $\nabla \cdot (\mathbf{u}'\phi')$ stems from averaging processes applied to the hyperbolic term ($\mathbf{u} \cdot \nabla\phi$, see Vallis (2017)). We believe that the term $\nabla \cdot (\mathbf{u}'\phi')$ smears out the mean value of ϕ, and smearing is also what the closure from eq. 2.8 does. With the right choice of κ this closure might give the right steady state tracer distribution for our system, but the transition times might be different: When we run a model in a coarse resolution, there might be parts of the domain, where no wave modes are excitable, and only the diffusion term can be excited. This could be different for higher resolutions, where eddies can be excited. This will be tested in section 4.6.

When we in the next chapter are looking for signal propagation speeds, we have to keep in mind, that our system might occasionally be parabolic, and therefore allow for very fast signal propagation.

3   Model domain and setup
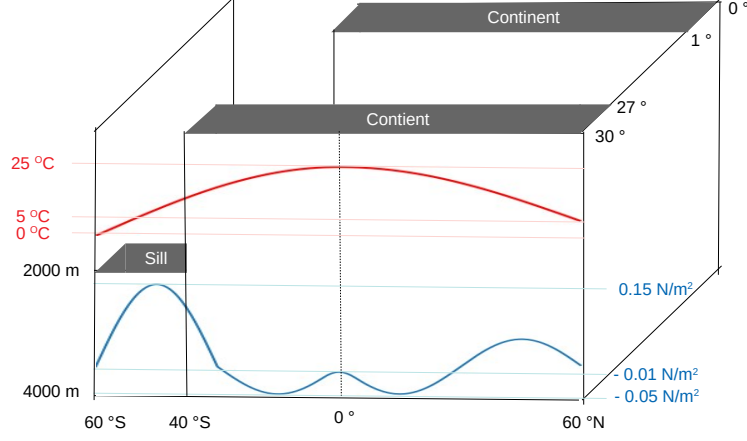
Figure 3.1: *The model consists of a basin that spans from $40°$ S to $60°$ N, and a channel in the southern part. The channel has a sill to resemble the Drakes passage.*

To address these questions a model (we use VEROS (Häfner et al. (2018)), a purely python based model) that resembles that of Munday et al. (2012) is used (see Fig 3.1). The domain spans from $60°$ south to $60°$ north, and $30°$ east-west. The depth is 4000 m, but with a sill of depth 2000 m located south of $40°$ S. The sill gives rise to periodic boundary conditions in the upper half of the southern part of the domain, and the setup is therefore a combination of both a basin and a (periodic) channel. This is to mimic the Atlantic basin together with Drakes' passage and the SO. The model uses a TKE-model as described in Gaspar et al. (2008). The parameters used can be found in table 3.1. The forcing applied to the model can be seen in Fig. 3.1.

The upper surface is forced by a zonal wind stress given by

$$\tau_x(\theta) = 10^{-4}\rho \cdot \begin{cases} 1.5\sin\left(\pi\frac{\theta+60°}{30°}\right), & \text{if } \theta < -30° \\ -0.5\sin\left(\pi\frac{\theta-30°}{30°}\right), & \text{if } -30° < \theta < -5° \\ 0.15\cos\left(\pi\frac{\theta-10°}{10°}\right) + 0.25, & \text{if } -5° < \theta < 5° \\ 0.5\sin\left(\pi\frac{\theta-30°}{30°}\right), & \text{if } 5° < \theta < 30° \\ -0.5\sin\left(\pi\frac{\theta-60°}{30°}\right), & \text{if } 30° < \theta \end{cases} \quad (3.1)$$

The surface is relaxed to a temperature profile given by

$$T^*(\theta) = \begin{cases} T_s + \Delta T\sin\left(\pi\frac{\theta+60°}{120°}\right), & \text{if } \theta < 0° \\ T_n + (\Delta T + T_s - T_n)\sin\left(\pi\frac{\theta+60°}{120°}\right), & \text{if } 0° < \theta, \end{cases} \quad (3.2)$$

8

with $T_s = 0\,°\text{C}$, $T_n = 5\,°\text{C}$ and $\Delta T = 25\,°\text{C}$. The relaxation constant is found in table 3.1. The north-south asymmetry with $5°\text{C}$ higher temperature in the North is to mimic the temperature difference between the areas of deep convection in the North Atlantic and the southern most part of the SO.

Parameter	Symbol	Value	Units
Vertical viscosity	ν_v	variable	m^2/s
Horizontal viscosity	ν_h	10^5	m^2/s
Time step	Δt	3600	s
Restoring timescale, salt	τ_S	30	days
Restoring timescale, temperature	τ_T	10	days
Horizontal resolution	-	2	$°$
Vertical resolution	-	variable with 40 layers	-

Table 3.1: Model parameters used in simulation

To address question 4, we set up a small ensemble of models with each of the three members having different κ. The chosen values of κ are $\kappa_{500} = 500\,\text{m}^2/\text{s}$, $\kappa_{1000} = 1000\,\text{m}^2/\text{s}$ and $\kappa_{2000} = 2000\,\text{m}^2/\text{s}$. The models are spun up for 600 model years.
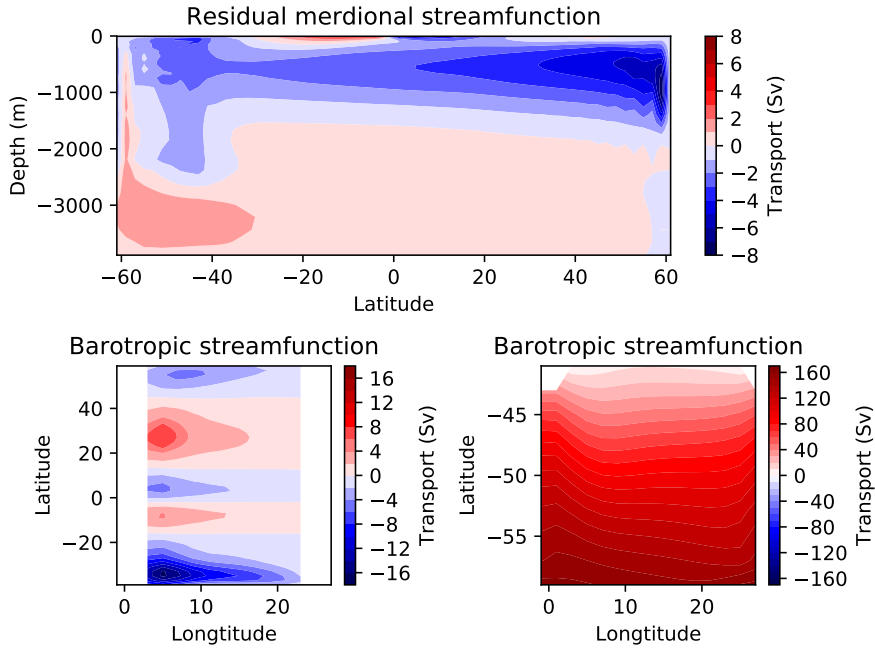
Figure 3.2: *Barotropic and residual meridional streamfunction (RMS) for the spun-up model for κ_{500}. The RMS shows a hemisphere crossing overturning cells in both the upper (fed by deep water from the north) and lower (fed with water from most southern part of the channel) part of the basin. The barotropic streamfunction shows wind-driven cells and and a zonal current in the periodic channel.*

After this spin-up phase the circulation has four wind-driven cells (two in each hemisphere, see Fig. 3.2) and a current resembling the ACC flowing in the periodic channel.

Also the circulation has a clear meridional overturning (MOC) with deep-water formation in the north and lift of deep water in the channel. The circulation also has a deep cell fed by water from the very south of the channel.

To be able to answer our questions we now change our forcing so that we generate 5 branches of our ensemble:

(a) In the first branch - which members are called **-SALT*n***, where $n = $ ***500, 1000, 2000*** depending on κ - the salinity in the very north is relaxed towards a lower value: From $50°$ N to $60°$ N the salinity is gradually lowered from $S_n = 35$ PSU to 34 PSU. The relaxation profile is given by

$$S^*(\theta) = \begin{cases} S_n, & \text{if } -50° < \theta \\ S_n + \sin\left(\frac{-\pi}{2}\frac{50-\theta}{10°}\right), & \text{if } \theta < -50°. \end{cases} \quad (3.3)$$

The relaxation constant is found in table 3.1. This resembles the perturbation of Pedro et al. (2018), and will help us address question 4 from chapter 1.

(b) In the second branch - members called **SALTEQ*n*** - the salinity is also relaxed as described by eq. 3.3, and the winds over the equator are turned off:

$$\tau_x(\theta) = 0, \text{ for } -5° < \theta < 5°. \quad (3.4)$$

This perturbation will help us address question 2 from chapter 1.

(c) In the third branch - members called **SALTSO*n*** - the salinity is also relaxed, and the winds over the channel are moved slightly south:

$$\tau_x(\theta) = 10^{-4}\rho \cdot \begin{cases} 1.5\sin\left(\pi\frac{\theta+60°}{28°}\right), & \text{if } \theta < -32° \\ -0.5\sin\left(\pi\frac{\theta-30°}{30°}\right), & \text{if } -32° < \theta < -15° \end{cases} \quad (3.5)$$

This corresponds to moving the wind peak over the channel $1°$ south. This perturbation will help us address question 3 from chapter 1.

(d) The fourth branch has no salinity relaxation - called **OSO*n*** - and only the winds over the channel are moved slightly south as described by equation 3.5. This will also help us to address question 3 from chapter 1.

(e) In a fifth branch - **+SALT*n*** - the salinity in the North is nudged towards a higher value (36 PSU), when going from $50°$ N to $60°$ N. This perturbation will help us address question 5 from chapter 1.

These 16 ensemble members are integrated for another 400 model years, and the output is compared to before the branching. As control, a sixth branch with no changes is

also integrated for another 400 model years, and this unchanged branch did not evolve during this time.

A high ($1/6°$) resolution model called **-SALT***H* of the same domain was integrated for 30 years spin-up. After this short spin-up the same fresh water perturbation as described above was applied, and the model ran for another 30 years. The high resolution model has $\kappa = 0.26\,\mathrm{m^2/s}$, time steps is $\Delta t = 600\,\mathrm{s}$, and we have introduced a biharmonic viscosity of $10^{10}\,\mathrm{m^4/s}$. An unperturbed control showed $\sim 5\%$ cooling doing the 20 years.

4 Analysis of model results

First we consider the consequences of the perturbation applied to **-SALT*n***, which is a fresh water leak at high northern latitude.
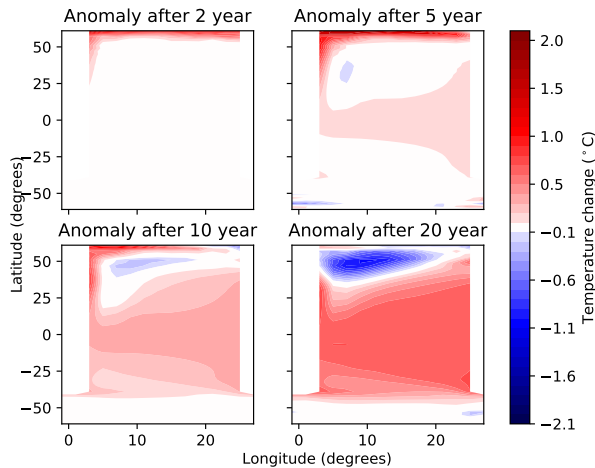
Figure 4.1: *Temperature anomaly for **-SALT500** in 500 m depth. The equator and boundaries first heat up due to kelvin waves. The interior warms due to Rossby waves.*

4.1 Collapse of the overturning

The strength of the overturning decreases significantly, when fresh water is released. To quantify this we use the same metric as Jochum and Eden (2015) (See table 4.1). We see that the decrease in the overturning is insensitive to our choice of κ, but that the initial and final strength of the overturning is sensitive to κ.

Branch	Before leak	After leak	change
-SALT*500*	2.9 Sv	1.6 Sv	-1.3 Sv
-SALT*1000*	2.4 Sv	1.0 Sv	-1.4 Sv
-SALT*2000*	1.6 Sv	0.3 Sv	-1.3 Sv
-SALT*H*	3.8 Sv	1.2 Sv	-2.6 Sv

Table 4.1: Changes in the overturning defined as the maximum value of the overturning streamfunction (see Fig. 3.2) below 300 m depth at the equator. (See Jochum and Eden (2015)). *Calculated after 30 years, not after 400 years

On the contrary, the circulation in the channel is independent on the value of κ and is insensitive to the fresh water perturbation (See table 4.2).

12

Branch	Before leak	After leak	Changes
-SALT*500*	3.5 Sv	3.3 Sv	-0.2 Sv
-SALT*1000*	3.6 Sv	3.5 Sv	-0.1 Sv
-SALT*2000*	3.7 Sv	3.7 Sv	0.0 Sv

Table 4.2: Changes in Southern ocean circulation defined as the maximum value over the overturning stream function south of 40 ° S.

4.2 Propagation of the temperature anomaly
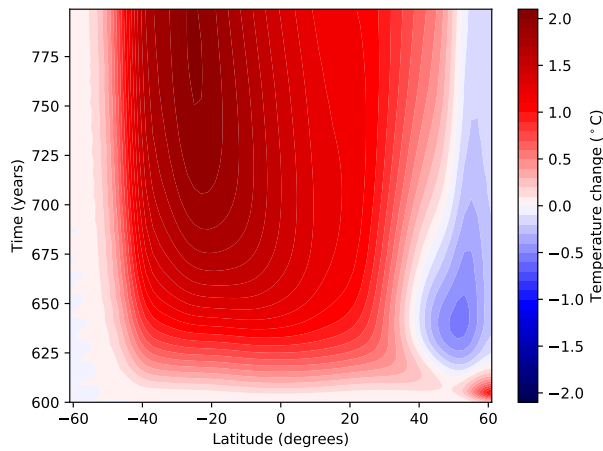
Figure 4.2: *Hovmöller diagram for the zonally averaged temperature at 500 m depth (here for **OSALT** and κ_{500}). A wave signal is seen the first 5 years. After this a slower diffusive signal is seen in the channel ($40°$ to $60°$ S).*

To analyze the effect of the perturbation on the temperature distribution in the ocean, a temperature anomaly is calculated as the difference between the fresh water perturbed models and the unperturbed model. For the branch **-SALT*n*** the temperature anomaly develops in qualitatively the same way for all values κ, and the initial phase shares a number of key features with the description by Kawase (1987): When fresh water starts being leaked, a warm Kelvin wave starts to propagate from the north to the equator along the western boundary. When it reaches the equator, it travels along the equator, and when the eastern boarder is reached, the wave splits up and propagates both north and south. The Kelvin wave radiates Rossby waves, that deepens the thermocline in the basin. This development is seen in Fig 4.1. The temperature signal for all values of κ is strongest around 500 m depth. The overall result is a deepening of the thermocline in the ocean basin.

The time it takes for the signal to arrive in the channel is quite independent of κ (3-4 years, Fig. 4.5), and as soon as the channel is reached, the temperature starts to rise in all of the channel.

Though a small temperature change can be noticed in the channel early, the heat transport is less efficient in the channel compared to the basin. This is seen in a Hovmöller diagram (Fig. 4.2).

When the integration is done, the ocean interior and surface has warmed, and it is only at high northern latitude that a cold anomaly is seen. This can be seen in the latitude-depth plot in Fig. 4.3. Although a temperature increase can be noticed in all of the channel, Fig. 4.3 suggests that the majority of the heat is confined and arrested above a certain latitude within the channel. For a lower κ, the signal is arrested at a lower latitude.

From Fig. 4.3 we also see that the temperature anomaly follows the isopycnals almost to the out crop point. This tells us that the heat's ability to penetrate in channel is limited by isopycnals. As seen in Fig. 4.4, this is the case for all values of κ.

Further transport of heat would require a new mechanism, which Pedro et al. (2018) found to be melting of sea ice.
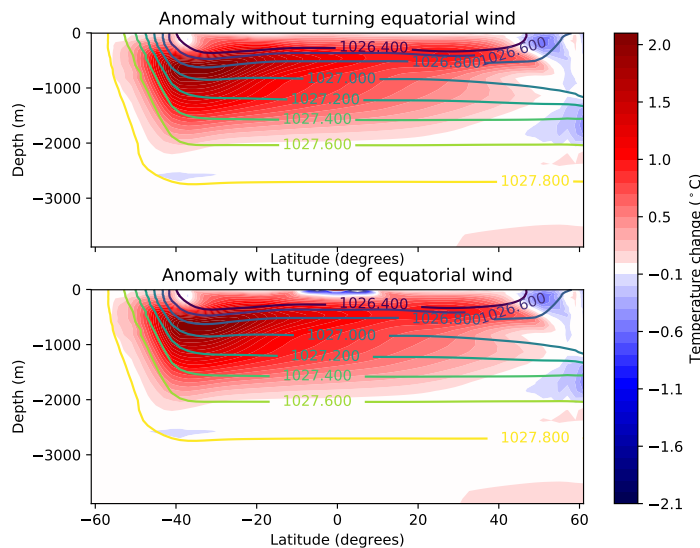
Figure 4.3: *Zonal average of the temperature anomaly after 400 years. The upper figure shows **-SALT500**. The lower figure **SALTEQ500**. We see that these two only differ in the surface layer right at the equator. In the southern hemisphere, the temperature anomaly follows isopycnals almost all the way to the outcrop point, where the anomalies bend northward. Contour lines show isopycnals.*

4.3   Heat accumulation in the ACC

The next question is how much heat is accumulated in the channel. For all branches and ensemble members a time series of the average temperature is calculated between 100 m and 700 m depth and $42°$ S to $51°$ S (Fig. 4.5).

We see that the change in temperature depends on κ, so that lower κ, means higher temperature increase. As we have seen already there is a small dependency on whether or not we change the winds over the channel. The change in wind over the equator do not induce any change in the channel at all.

Fig. 4.5 shows that the time it takes for the signal to arrive in the channel is quite independent of κ (3-4 years). This is no surprise since the signal arrives in the channel by means of wave transport and not eddy diffusion.

As soon as the wave has reached the channel, a temperature increase can be noticed all across the channel. The temperature increase saturates over time. The timescale (e-folding time) of the temperature anomaly growth is rather independent of κ (26.1-28.9 years, Fig. 4.5). This contrasts the magnitude of the response which decreases with κ. It also contrasts the intuition one could have, that a larger diffusivity means a faster response. Here it is worth noting, that the temperature flux from the parameterized eddies doesn't depend solely on the diffusion coefficient and the temperature gradient, since it's anti-symmetric part also depends on the slope of the isopycnals (Griffies (2003)). As we see from Fig. 4.4 the high κ also have the most horizontal slope of the temperature anomaly field and the density field. This decreases the response time. This is the same conclusion as in section 2.3, where we from dimensional arguments arrive at a time scale of the same order of magnitude as from the numerical experiments described here.

4.4 Effects of wind changes
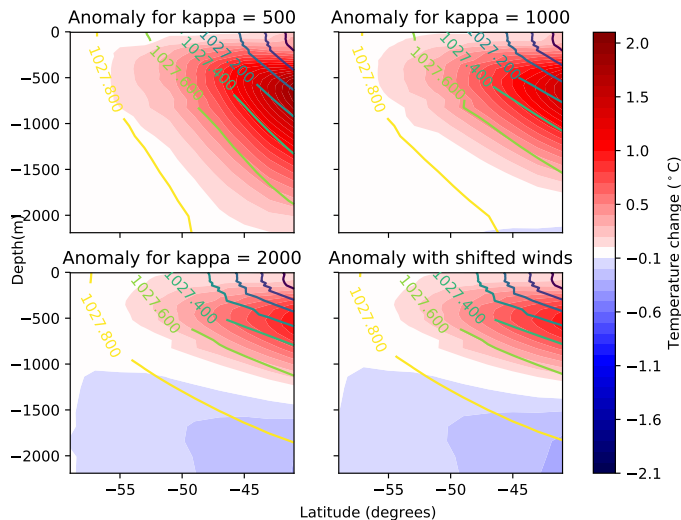
Figure 4.4: *Location of the temperature anomaly after 400 years for **-SALTn**, and for **SALTSO2000**. The signal is always arrested by isopycnals. A southward shift of the wind doesn't change the location of the anomaly or the structure of the isopycnals.*

To turn of the wind at the equator (**SALTEQ*n***) doesn't change the response time or the magnitude of the temperature change in the channel. This can be seen in Fig. 4.5 and 4.3. The change of the equatorial wind only induces some local changes in the surface layer at the equator.

Changing the wind over the channel in **SALTSO*n*** does induce some effects. It pushes the temperature anomaly a little further south ($0.5°$, so less than the southward movement of the wind stress maximum).

The wind change in the channel does also give a small increase in the channel temperature (see Fig. 4.5), but this is all minor compared to the fresh water perturbation (9 % for κ_{500}, $> 1\%$ for κ_{2000}. Identified from the location of the 0.2 C$°$ temperature anomaly). Also the temperature anomaly is almost identical with and without changes in the channel wind (Fig. 4.4).

The heating induced from only changing the wind over the channel (branch 4) and not releasing fresh water seems very small and decays over time (Fig. 4.5).
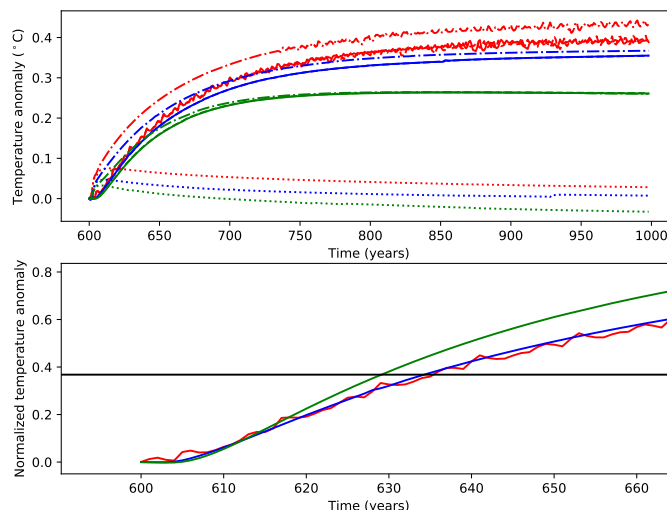
Figure 4.5: *The upper figure shows the temperature anomaly from 100 m to 700 m depth between 42 $°$ S and 51 $°$ S for κ_{500}, κ_{1000} and κ_{2000}. The solid lines show -SALTn the $- \cdot -$ dashed lines are SALTOSn, and the $\cdots$ dashed lines show OSOn. The figure also shows SALTEQn, but these lines coincide with those of OSALT, and are therefore hard to see. The lower figure shows the initial phase of the warming with normalized values (divided by their maximum value) for -SALTn.*

4.5 Asymmetry of fresh and salt water perturbations

The response of our ocean-only model to a fresh water perturbation does mimic that of Pedro et al. (2018) independent of whether the wind is changed or not. We would also
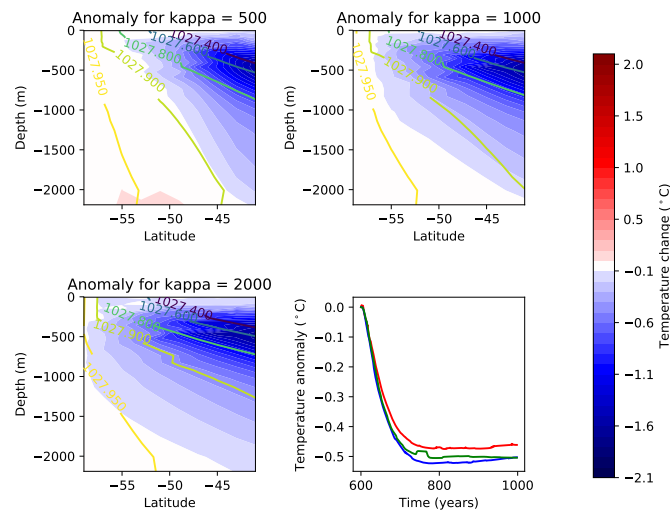
Figure 4.6: *The figure shows the temperature anomaly after 400 years for **+SALTn**. The lower left figure shows a time series of the temperature anomaly in the northern half of the channel. Just like for **-SALTn** the response time for the temperature change in the channel is independent of κ, but unlike **-SALTn**, the magnitude of the response is also independent. In contrast to **-SALTn** a higher κ means a further southward propagation of the temperature anomaly. There is a tendency for the anomaly to cross isopycnals. Contour lines show isopycnals.*

like to know if our model is symmetric in its response to salt and fresh water perturbation. If one compare Fig. 4.4 and Fig. 4.5 to Fig. 4.6, one finds that they are quite similar, but they also show some differences: For the highest κ the temperature anomaly makes it furthest to the south, whereas this was the opposite for the fresh water perturbation. Actually the κ_{2000} makes it almost to the southern border of the channel for **+SALTn**. The cause for this asymmetry is not clear, but a part of the explanation might be found in another tracer field, the salinity field: First of all, the salt water perturbation strengthens the overturning. This advects the salt anomaly all the way to the southern border (Fig. 4.7), which means that temperature is no more the only density controlling tracer in the channel. This is in contrast to the fresh water case, where the salt anomaly never makes it to the channel. The more dense water now formed in the North gives rise to new adiabatic pathways to the south, and more dense isopycnals now outcrop in the channel.

The co-existence of salinity and temperature anomalies make it possible for baroclinic eddies to move heat across isopycnals in an adiabatic way. But not only adiabatic processes could be important, also diabatic ones could matter here: From Fig. 4.6 and 4.7 we see that the temperature signal crosses the isopycnals where the salinity perturbation is small (above 400 m depth). Here deep cold water meets cold surface water, so the density gradient is much smaller then for **-SALTn**, and it is therefore easier for the wind to induce cross-isopycnal mixing in the upper part of the ocean, which could be what progresses the

signal so far south.

Here it is important to remember that if a fresh water perturbation is now induced on top of the salt water perturbation, we would see a withdrawal of cold temperature anomaly, and the effects of the fresh water perturbation would in this case reach all the way to the southern border, only since we now can communicate through denser isopycnals.

The response is otherwise similar to **-SALT*n***: The magnitude of the anomaly is rather independent of κ for **+SALT*n*** (0.47 - 0.53 $^\circ C$) and of similar size to **-SALT*n*** (0.22 - 0.36 $^\circ C$). The response time is also similar (4 years for the waves to make it to the channel, and 27.1 years response time for κ_{2000} and κ_{1000}, and 29.9 years for κ_{500}. The response time was 26.1-28.9 years for fresh water). Again we see that the size of the diffusivity, κ and the isopycnal slope balance out each other, so that we get a response time that is independent of κ - and also independent of whether the sign of the perturbation.
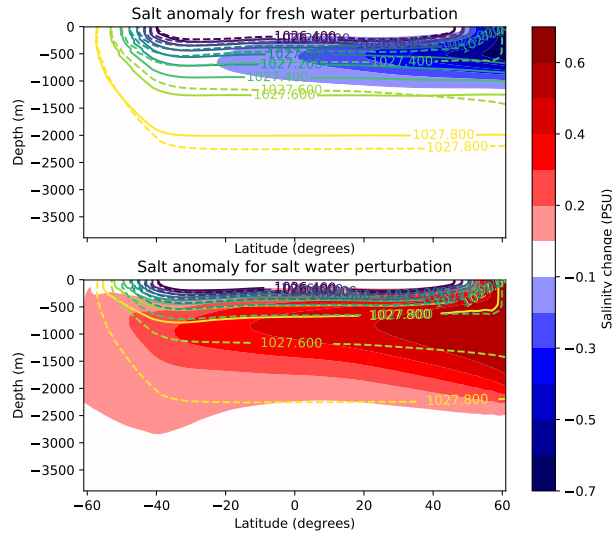
Figure 4.7: *Salinity anomaly profile 400 years after the perturbations are applied. The upper part shows **-SALTn** and the lower part shows **+SALTn**. We see that salinity changes propagate further south **+SALTn**. This means that for **+SALTn** both temperature and salinity are dynamical tracers in the Channel. Contour lines show isopycnals.*

4.6 High resolution run

The high resolution run, **-SALT*H***, partially develops in the same way as **-SALT*n***. The overturning is much stronger after the 30 years of spin-up, then it is for any of the coarse resolution runs (table 4.1). The response to the perturbation however develops in a similar way: After the fresh water perturbation is applied, Kelvin waves starts to travel southwards (compare Fig. 4.8 to Fig. 4.1). The Kelvin waves are weaker and faster then for

-SALT*n*, and already after 1 year, the development of Rossby waves can be seen at the eastern boundary (Fig. 4.8). The developing Rossby waves are easy to spot compared to the Kelvin wave. This contrast **-SALT*n***, where the Kelvin waves are more prominent. The relative weakness of the Kelvin waves makes them difficult to spot. We explain this phenomena by the refraction of Kelvin into Rossby waves at the eastern boundary: The Rossby waves move slow compared to the Kelvin waves, and they therefore have time to pick up a lot of signal before they leave the eastern boundary and start to travel westward. The Rossby waves are seen most clearly between $\sim 10°$ and $\sim 25°$. This fits well from observations in the ocean (Lacasce and Pedlosky (2004)). This has been explained by the higher speed of Rossby waves at low latitude (Lacasce and Pedlosky (2004), due to higher β and a phase shift in the subtropical gyre), and likewise slower growth of instabilities (due to smaller f, Vallis (2017)).
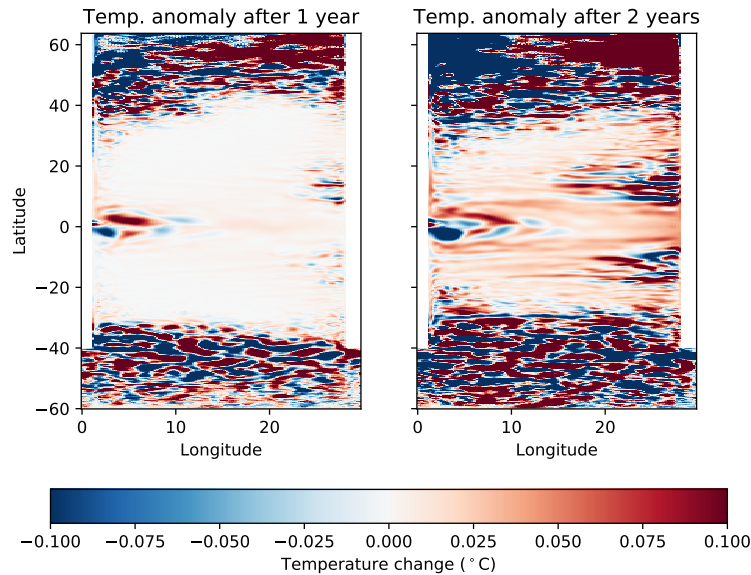
Figure 4.8: *Temperature anomaly in upper 300 m for the initial phase for **-SALTH***. *A Kelvin wave is seen as a narrow and light red stripe at the western boundary in the northern hemisphere after 1 year. The Kelvin wave can also be recognised at equator and the eastern boundary. At the eastern boundary Rossby waves are slowly building up. After two years the Roosby waves has moved further into the bassin.*

After 30 years the ocean has warmed up in a way similar to **-SALT*n***, and the strength of the overturning has reduced drastically. As shown in Fig. 4.9 we see a cold anomaly in the very north and heating in the rest of the basin. The channel shows are more complicated pattern then was the case for the coarse resolution runs. Here we see patches of both cold and warm anomalies. We belive that this stems from eddy activity in the channel. Excitation of eddies was not possible for the runs with coarser resolution. Fig. 4.9 shows

that **-SALT*H*** has deeper isopycnals than the **-SALT*n*s**. The best agreement however is with **-SALT*500***. If this has to do with the reduced spin-up time or has an actual dynamical explanation is not clear.
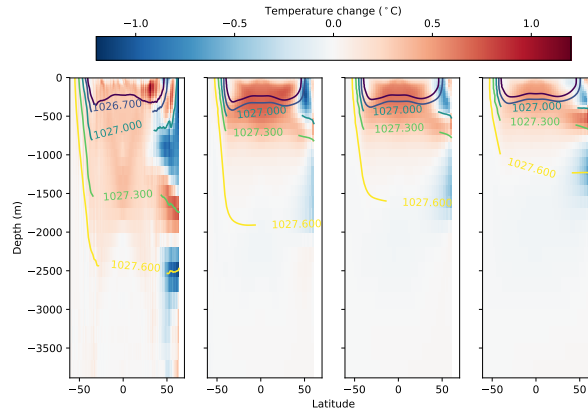
Figure 4.9: *Cross section average temperature anomaly 20 years after the perturbation for (from left to right) **-SALTH, -SALT500, -SALT1000** and **-SALT2000**. Contour lines show isopycnals.*

The better agreement with **-SALT*500*** seems also to be the case for the development of the channel temperature (Fig 4.10), though a lot of noise and a short integration time complicates the picture. From Fig. 4.10 one could even think that the response for the high resolution model is stronger and faster then for any of the coarse resolution cases - just like the overturning also was stronger (table 4.1). But before making this conclusion it is important to bear in mind that due to short spin up time, the unperturbed control run of **-SALT*H*** shows a temperature drift of $\sim 5\%$. This is more then the $\sim 1\%$ change in the channel temperature arising from the perturbation.
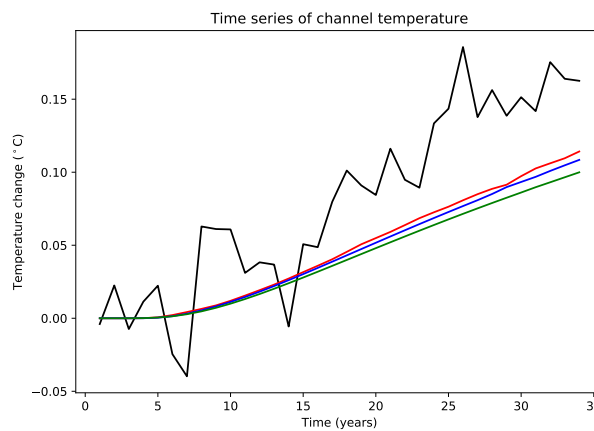
Figure 4.10: *The figure shows the temperature anomaly from 100 m to 700 m depth between 42 ° S and 51 ° S for **-SALT500**, **-SALT1000**, **-SALT2000** and **-SALTH**.*

5 Summary and Discussion

In this thesis a salinity perturbation is applied at high northern latitude in an idealised model of the Atlantic basin and the Southern Ocean. The model consists of a basin and a channel, and is forced by a temperature relaxation profile and a constant wind profile (see Fig. 3.1).

The salinity perturbation gives rise to a southward traveling temperature signal: A warm signal, when the perturbation is fresh. A cold signal, when the perturbation is salt. The propagation can be decomposed into two parts: A fast part in the basin that consists of Kelvin and Rossby waves. And a slow part of temperature diffusion through the channel. The signals ability to penetrate isopycnals was limited.

The study concerns the time it take the signal from the salinity perturbation to travel from high northern latitudes to high southern latitudes. This has been investigated in a number of different setups, where the salinity perturbation was accompanied with changes in other conditions: A $1°$ southward shift of the winds over the channel (corresponding to the westerlies), a turn-off of the winds over the equator, the value of the eddy diffusivity constant and whether the salinity perturbation is salt or fresh. We found that travel time of the signal was independent of wind changes at the equator. This is in agreement with the classical theories of Pedlosky (1991) and Pedlosky (1987). The heat content of the entire domain also seems to be mostly independent of the equatorial wind perturbations, since the removal of wind at the equator only induces a change in the upper part of the ocean, right at the equator.

The $1°$ southward wind shift did push the signal $0.5°$ further south, however since the signal shift is smaller then the shift of the wind itself, this can be considered a minor change. The response time of the signal was unaltered by the southward shift of the wind.

Both the wave travel time ($\sim$4 years) in the basin and the eddy response time ($\sim$27 years) in the channel were similar for all values κ. This is in agreement of the scale analysis of section 2.3, and the time scale fits well with the indication of a short integration of a high resolution model. On the contrary the magnitude of the temperature change did depend on κ, with a low κ giving the largest response.

The thermocline depth, and hence the magnitude of the ocean heating is depending on κ: A high κ gives a shallow thermocline and a smaller warming, where as a low κ gives a deep thermocline and a larger warming. This is only the case for the fresh water perturbation. For the salt water perturbation, the magnitude of the temperature change was found to be independent of κ. On the contrary, the response time was in the same range for both fresh and salt perturbations.

5.1 Questions of chapter 1 - the effect of wind changes on oceanic adjustments

Returning to the questions inspired by Pedro et al. (2018) and their coupled model, we now have indications that the timescales they find in the Atlantic basin are due to Kelvin and Rossby waves and not to the changes in the atmospheric circulation.

From our results the warming in the Southern Ocean noted by Pedro et al. (2018) could be rather independent of the southward shift in the southern hemisphere westerlies found in the same study. These wind changes might of course be important for the transport of heat to the Antarctic continent, but for the heat content in the Southern Ocean our study suggest them to be of minor importance. Generally our study suggest a partial decoupling of the ocean signal propagation from the atmosphere outside of the highest latitudes.

This can be summarized by answers to the questions of chapter 1:

1. *Pedro et al. (2018) find that the salinity perturbation in the North Atlantic induces both changes in the atmospheric circulation and heat content of the ocean. The change in the oceanic heat content might be due to direct adjustment to the salinity perturbation. It might also have an indirect contribution from oceanic response to the wind changes. How do the direct and indirect contribution compare?*

   Our experiment indicates that direct oceanic response to the salinity perturbation accounts for the vast majority of the heating found by Pedro et al. (2018)

2. *Pedro et al. (2018) finds that the zonal wind over the equator decreases in strength. How does it effect the travel time of the signal from the fresh water perturbation?*

   We find that the wind changes over the equator doesn't change the time scale of the adjustment

3. *The winds over the ACC move slightly south in Pedro et al. (2018)'s study. How does this effect the travel time of the signal from the fresh water perturbation?*

   We find that the wind changes over the channel doesn't change the time scale of the adjustment

4. *How does the travel time of signal depend on κ?*

   The time scale is independent of κ, and the time scale is found to agree with a high resolution run and with a scale analysis

5. *Is the response symmetric to the sign of the salinity perturbations?*

   The time scale of the response is independent of the sign of the salinity perturbation.

6. *Does the travel time change with improved resolution?*

   The response time seems to stay unaltered by the improved resolution, though it might be a little faster.

5.2   Estimation of κ from ice cores

Our study was initially meant to investigate the coupling of different parts of the earth system in the response of a salinity perturbation. The salinity perturbation was chosen to mimic the changes if the transition of Dansgaard-Oeschger events. As explained above we find that the ocean adjustment to the salinity perturbation is insensitive to the accompanying atmospheric adjustment.

Our experiment could also be a way to estimate κ from the very long time series the Greenland ice cores spans. This should be done from finding the κ that made the response time fit that from ice core best (WAIS Divide Project Members (2015); Buizert et al. (2018)).

A surprising finding is that the response time is independent of κ. This goes for both the eddy and the wave signal. The response time is the same as we find by a scale analysis and consistent with the indications from a short integration of a high resolution model.

The speed and nature of boundary waves in ocean models are known to differ in different ocean models(Marshall and Johnson (2013)), but κ doesn't seem to have an impact on this.

Unfortunately the timescales we find are an order of magnitude shorter then the time lag found by WAIS Divide Project Members (2015) and Buizert et al. (2018) ($\sim$30 years including both waves and diffusive processes vs. $\sim$200 years), and even more importantly our timescales (excluding the wave part) do not even represent a lag. A similar discrepancy is seen in Schmittner et al. (2003) and Pedro et al. (2018). In the channel our coarse resolution doesn't allow for waves or eddies to be easily excited, and only eddy diffusion might come into play. Since the GM eddy diffusive closure is parabolic, the transport it causes might give unrealistically fast responses (Durran (2010); Landau and Lifshitz (1966)). However our short integration of a high resolution setup indicates, that this is not the case. Poulsen et al. (2018) found that the steady state tracer distributions of GM-dependent models are in agreement with eddy resolving models, and our findings indicate that that adjustment timescales found by GM-dependent models and eddy resolving models are also in agreement.

5.3   What causes the time lag found in ice cores?

We now have indications that the time scales for the adjustments of the Southern Ocean to the salinity perturbation are independent of the adherent wind changes, but we also have indications that the oceanic timescales alone can't account for the delayed found by Buizert et al. (2018) and WAIS Divide Project Members (2015). We therefore suggest that other mechanisms have to explain parts of the lag. This could be melting and formation of sea ice.

Bibliography

Buizert, C., M. Sigl, M. Severi, B. R. Markle, J. J. Wettstein, J. R. McConnell, J. B. Pedro, H. Sodemann, K. Goto-Azuma, K. Kawamura, S. Fujita, H. Motoyama, M. Hirabayashi, R. Uemura, B. Stenni, F. Parrenin, F. He, T. J. Fudge, and E. J. Steig 2018. Abrupt ice-age shifts in southern westerly winds and Antarctic climate forced from the north. *Nature*, 563(7733):681–685.

Durran, D.
2010. *Numerical Methods for Fluid Dynamics With Applications to Geophysics*.

Eden, C., M. Jochum, and G. Danabasoglu
2009. Effects of different closures for thickness diffusivity. *Ocean Modelling*, 26(1-2):47–59.

Ferrari, R. and M. Nikurashin
2010. Suppression of eddy diffusivity across jets in the Southern Ocean. *Journal of Physical Oceanography*, 40(7):1501–1519.

Ferreira, D., J. Marshall, and P. Heimbach
2005. Estimating Eddy Stresses by Fitting Dynamics to Observations Using a Residual-Mean Ocean Circulation Model and Its Adjoint. *Journal of Physical Oceanography*.

Gaspar, P., Y. Grégoris, and J.-M. Lefevre
2008. A simple eddy kinetic energy model for simulations of the oceanic vertical mixing: Tests at station Papa and long-term upper ocean study site. *Journal of Geophysical Research*.

Gent, P. and J. Mcwilliams
1990. Isopycnal Mixing in Ocean Circulation Models. *Journal of Physical Oceanography*, 20.

Gent, P., J. Willebrand, T. McDougall, and J. McWilliams
1995. Parameterizing Eddy-Induced Tracer Transports in Ocean Circulation Models. *Journal of Physical Oceanography*, 25(4).

Griffies, S. M.
1998. The Gent–McWilliams Skew Flux. *Journal of Physical Oceanography*, 28(5):831–841.

Griffies, S. M.
2003. *Fundamentals of Ocean Climate Models*.

Häfner, D., R. L. Jacobsen, C. Eden, M. R. Kristensen, M. Jochum, R. Nuterman, and
B. Vinter
2018. Veros v0.1 - A fast and versatile ocean simulator in pure Python. *Geoscientific Model Development*, 11(8):3299–3312.

Jochum, M. and C. Eden
2015. The connection between Southern Ocean winds, the Atlantic Meridional overturning circulation, and Indo-Pacific upwelling. *Journal of Climate*.

Kawase, M.
1987. Establishment of Deep Ocean Circulation Driven by Deep-Water Production. *J. Phys. Oceanogr.,*, 17:2294–2317.

Kuhlbrodt, T., A. Griesel, M. Montoya, A. Levermann, M. Hofmann, and S. Rahmstorf
2007. On the driving processes of the Atlantic meridional overturning circulation. *Reviews of Geophysics*.

Kuhlbrodt, T., R. S. Smith, Z. Wang, and J. M. Gregory
2012. The influence of eddy parameterizations on the transport of the Antarctic Circumpolar Current in coupled climate models. *Ocean Modelling*, 52-53:1–8.

Lacasce, J. H. and J. Pedlosky
2004. The Instability of Rossby Basin Modes and the Oceanic Eddy Field *. *Journal of Physical Oceanography*.

Landau, L. D. and E. M. Lifshitz
1966. *Fluid Mechanics*.

Marshall, D. P. and H. L. Johnson
2013. Propagation of meridional circulation anomalies along western and eastern boundaries. *Journal of Physical Oceanography*, 43(12):2699–2717.

Marshall, J., E. Shuckburgh, H. Jones, and C. Hill
2006. Estimates and Implications of Surface Eddy Diffusivity in the Southern Ocean Derived from Tracer Transport. *Journal of Physical Oceanography*, 25.

Munday, D. R., H. L. Johnson, and D. P. Marshall
2012. Eddy Saturation of Equilibrated Circumpolar Currents. *Journal of Physical Oceanography*.

Nielsen, S. B., M. Jochum, J. B. Pedro, C. Eden, and R. Nuterman
2019. Two-Timescale Carbon Cycle Response to an AMOC Collapse. *Paleoceanography and Paleoclimatology*, 34(4):511–523.

Nikurashin, M. and G. Vallis
   2011. A theory of deep stratification and overturning circulation in the ocean. *Journal of Physical Oceanography*, 41(3):485–502.

Pedlosky, J.
   1987. An Inertial Theory of the Equatorial Undercurrent. *Journal of Physical Oceanography*, 17.

Pedlosky, J.
   1991. A Link between Western Boundary Currents and Equatorial Undercurrents. *Journal of Physical Oceanography*.

Pedro, J. B., M. Jochum, C. Buizert, F. He, S. Barker, and S. O. Rasmussen
   2018. Beyond the bipolar seesaw: Toward a process understanding of interhemispheric coupling. *Quaternary Science Reviews*.

Poulsen, M. B., M. Jochum, and R. Nuterman
   2018. Parameterized and resolved Southern Ocean eddy compensation. *Ocean Modelling*.

Redi, M.
   1982. Oceanic Isopycnal Mixing by Coordinate Rotation. *Journal of Physical Oceanography*, 12.

Schmittner, A., O. A. Saenko, and A. J. Weaver
   2003. Coupling of the hemispheres in observations and simulations of glacial climate change. *Quaternary Science Reviews*.

Stocker, T. F. and S. J. Johnsen
   2003. A minimum thermodynamic model for the bipolar seesaw. *Paleoceanography*.

Vallis, G. K.
   2017. *Atmospheric and oceanic fluid dynamics: Fundamentals and large-scale circulation, second edition*.

WAIS Divide Project Members
   2015. Precise interpolar phasing of abrupt climate change during the last ice age. *Nature*, 520(7549):661–665.

A   Python code for data analysis

To generate the figure bellow, the following code is used
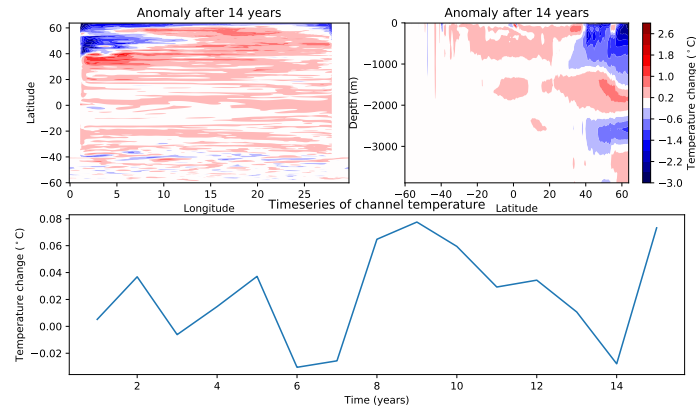

```python
import matplotlib.pyplot as plt
import matplotlib.patches as mpatches
import numpy as np
import matplotlib.gridspec as gridspec
from netCDF4 import Dataset
from scipy.integrate import trapz
from scipy.ndimage import gaussian_filter



radius = 6370e3   # Earth radius in m
degtom = radius / 180. * np.pi
mtodeg = 1. / degtom



vec_count =
    np.array([1115,1151,1187,1223,1259,
    1295,1331,1367,1403,1439,1475,1511,1547,1583,1619])

k = 2
```

```
with Dataset(
    "./control/acc_sector.hires.ctrl016." + str(vec_count[k])
        + ".averages.nc", "r") as datafile:
        xt = datafile["xt"][...]
        yt = datafile["yt"][...]
        zt = datafile["zt"][...]
        temp_ref = datafile["temp"][...]
    cosu = np.cos(yt * np.pi / 180.)



fig = plt.figure()
gs = gridspec.GridSpec(2, 2)

krav_x = np.logical_and(3 > xt, xt > 1)
krav_z = np.logical_and(0 > zt, zt > -300)



levels = [-3.0, -2.6, -2.2, -1.8, -1.4, -1.0, -0.6,
    -0.2, 0.2, 0.6, 1.0, 1.4, 1.8, 2.2, 2.6, 3.0]



with Dataset("./pert/acc_sector.hires.ctrl016."
    + str(vec_count[k]) + ".averages.nc", "r") as datafile:

        temp = datafile["temp"][...] - temp_ref
        h = temp[-1,:,:,:]
        h = h[krav_z,:,:]
        h = np.mean(h, axis = 0)

f_ax1 = fig.add_subplot(gs[0, 0])

im1 = f_ax1.pcolor(xt, yt, h, vmin = -0.1,
    vmax = 0.1, cmap = 'RdBu_r')
f_ax1.set_title('Anomaly after 14 years')
f_ax1.set_xlabel('Longitude')
f_ax1.set_ylabel('Latitude')
```

```python
with Dataset("./pert/acc_sector.hires.ctrl016."
    + str(vec_count[k]) + ".averages.nc", "r") as datafile:

        temp = datafile["temp"][...] - temp_ref
        h = temp[-1,:,:,:]
        h = h[:,:,krav_x]
        h = np.mean(h, axis = 2)
        rho = datafile["rho"][...] + 1024
        rho = rho[-1,:,:,:]
        rho = rho[:,:,krav_x]
        rho = np.mean(rho, axis = 2)



f_ax2 = fig.add_subplot(gs[0, 1])

im2 = f_ax2.pcolor( yt, zt, h, vmin = -0.1,
    vmax = 0.1, cmap = 'RdBu_r')



f_ax2.set_title('Anomaly after 14 years')
f_ax2.set_ylabel('Depth (m)')
f_ax2.set_xlabel('Latitude')

cbar2 = fig.colorbar(im2, ax=f_ax2)
cbar2.ax.set_ylabel('Temperature change ($^\circ$C)')



#Timeseries

with Dataset("./acc_sector.hires.ctrl016.1079.averages.nc",
    "r") as datafile:
        xt = datafile["xt"][...]
        yt = datafile["yt"][...]
        zt = datafile["zt"][...]
        temp_ref = datafile["temp"][...]


time_series = np.zeros((vec_count.size))
nx = xt.shape[0]
```

```python
ny = yt.shape[0]
nz = zt.shape[0]

krav_z = np.logical_and(0 > zt, zt > -300)
krav_y = np.logical_and(-42 > yt, yt > -50)
krav_x = np.logical_and(25 > xt, xt > 5)



temp_ref = temp_ref[-1,krav_z,:,:]
temp_ref = np.mean(temp_ref, axis = 0)
temp_ref = temp_ref[krav_y,:]
temp_ref = np.mean(temp_ref, axis = 0)
temp_ref = temp_ref[krav_x]
temp_ref = np.mean(temp_ref, axis = 0)



for i in range(vec_count.size):
        print(i + 1)
        with Dataset("./pert/acc_sector.hires.ctrl016." +
        str(vec_count[i]) + ".averages.nc", "r") as datafile:
                temp = datafile["temp"][...]
                temp = temp * cosu[np.newaxis,np.newaxis,
                    :,np.newaxis]
        h = np.mean(temp, axis=0)
        h = h[krav_z,:,:]
        h = np.mean(h, axis = 0)
        h = h[krav_y,:]
        h = np.mean(h, axis = 0)
        h = h[krav_x]
        h = np.mean(h, axis = 0)
        time_series[i] = h
        with Dataset("./control/acc_sector.hires.ctrl016." +
            str(vec_count[i]) + ".averages.nc", "r") as datafile:
                temp = datafile["temp"][...]
                temp = temp * cosu[np.newaxis,np.newaxis,
                    :,np.newaxis]
        h = np.mean(temp, axis=0)
        h = h[krav_z,:,:]
        h = np.mean(h, axis = 0)
```

```
        h = h[krav_y,:]
        h = np.mean(h,axis = 0)
        h = h[krav_x]
        h = np.mean(h,axis = 0)
        time_series[i] = time_series[i] - h




f_ax3 = fig.add_subplot(gs[1, :])

f_ax3.plot([1,2,3,4,5,6,7,8,9,10,11,12,13,14,15],time_series)

f_ax3.set_title('Timeseries_of_channel_temperature')
f_ax3.set_ylabel('Temperature_change_($^\circ$C)')
f_ax3.set_xlabel('Time_(years)')

plt.show()
```

B Unpublished article: Oceanic signal propagation from northern to southern high latitudes in the Versatile Ocean Simulator[1].

Abstract

The coupling between Dansgaard-Oescher events and Antarctic Isotope Maximas, together known as the bipolar seesaw, is a prominent example of interhemispheric teleconnection in the earth system. The bipolar seesaw has been reproduced in coupled earth system models, but it is still not clear which physical mechanisms facilitate this. The coupled models find changes in both ocean thermal structure and the atmospheric circulation, and their interdependence is not clear. To gain insight in this interdependence, we perturb an ocean general circulation model with a combination of salinity perturbations and changes in atmospheric forcing. These forcing changes are inspired by changes found in the coupled models, that simulate the bipolar seesaw. We find that the response time of the ocean thermocline to the salinity perturbations is insensitive to the changes in atmospheric forcing. We also find that the response time is insensitive to whether the salinity perturbation is fresh or salt, and to the magnitude of the eddy diffusion constant. We estimate that it takes the northern hemisphere anomalies several decades to cross the Southern Ocean, consistent with estimates from turbulent diffusion timescales but less then recently published estimates from proxy data.

B.1 Introduction

The climates of the two hemispheres of Earth are connected, most prominently seen in the comparison of Greenland and Antarctic temperatures (Stocker and Johnsen (2003)). During the last ice age sudden rises in Greenland temperature, the so called Dansgaard-Oescher events (DO), are followed by a delayed ($\sim$200 years, WAIS Divide Project Members (2015), Buizert et al. (2018)) and more gradual fall in Antarctic temperature, the so called Antarctic Isoptope Maxima (AIM). This overall covariation is known as the bipolar seesaw.

The explanation of the seesaw pattern by Stocker and Johnsen (2003) is that the Southern Ocean (SO) acts as a heat reservoir, that keeps heat when Greenland is cold and releases it when Greenland warms up. In Pedro et al. (2018), a coupled earth system model

---

[1]Submitted to Ocean Modelling 17/Oct/2019 by Laurits Støvring Andreasen, Markus Jochum and Roman Nuterman.
The figures are the same as in the thesis, but the caption might differ. The captions are found in section B.5.

33

is used to analyze the responses to fresh and salt water perturbations in the North Atlantic. These perturbations are suspected to have the same consequences as whatever mechanism triggers the stadial-interstadial transitions. Similar to the observed bipolar seesaw Pedro et al. (2018) finds that a fresh water perturbations in the North Atlantic lead to a delayed increase in Antarctic temperature. Some notable adjustment effects of the fresh water perturbation of Pedro et al. (2018) are a collapse of the Atlantic Meridional Overturning Circulation (AMOC), a weakening of equatorial winds, a southward shift of the westerlies over the SO, a deepening of the thermocline and melting of sea ice in the SO.

In the framework their coupled model it was not possible to determine unambiguously if the signal reached Antarctica solely through oceanic processes, or whether changes to equatorial or Southern Ocean winds play an important role in relaying the signal of northern hemisphere change. Thus, we will here use a forced ocean model to get a better understanding of the relevant oceanic processes. In particular we will investigate the time it takes the ocean signal to travel from high northern latitude to high southern latitude, and if it is influenced by atmospheric changes.

As argued by Kawase (1987), changes in ocean density in the northern hemisphere can be communicated along the equator and meridional boundaries by Kelvin waves to the other hemisphere. Furthermore, changes can effect the interior of a basin through westward Rossby waves emitted from the Kelvin waves. Note, though, that low frequency waves propagating along western and eastern boundaries are slightly different from classical Kelvin waves (Marshall and Johnson (2013)), but this doesn affect the reasoning behind Kawase (1987). Since Kawase's wave hypothesis requires meridional boundaries for any perturbation to travel south, it tells us little about how any pertubation can reach Antarctica from the north.

This was pointed by Schmittner et al. (2003), who suggest that baroclinic eddies in the SO must play a key role in the heat transport. Some effects of baroclinic eddies on the mean flow are to flatten isopycnals and to transport tracers along isopycnals (Gent et al. (1995)). The baroclinic eddies are not resolved in most ocean models used for climate studies, and are instead parameterized by isopycnal (Redi (1982)) and thickness diffusion (Gent and Mcwilliams (1990)). The strength of these respective diffusions depend on the slope of isopycnals and a parameter κ. Both a constant κ, and ones that vary in time and space are used in modelling (Eden et al. (2009)). Estimates of κ typically range from 300 m^{2}s^{-1} to 2000 m^{2}s^{-1} (Kuhlbrodt et al. (2012)).

The actual structure of κ is still a matter of debate, but at appears that at least for the Southern Ocean the ideas behind Ferreira et al. (2005) can reproduce much of the eddy effects seen in eddy resolving models (Poulsen et al. (2018)). To deal with the uncertainty in the value of κ we will perform the same experiments with different values of κ within the range of common values of climate models found by Kuhlbrodt et al. (2012).

The overall theme of this paper will be interhemispheric teleconnection. We will

perform an experiment similar to that of Pedro et al. (2018), where fresh and salt water is added in our model equivalent of the North Atlantic, and the questions we will address by this experiment, all inspired by Pedro et al. (2018), are:

1. What is the time it takes for North Atlantic signals to affect the Southern Ocean?

2. How important are North Atlantic buoyancy perturbations compared to equatorial and SO wind perturbations ?

3. How does the travel time of signal depend on κ?

4. Is the response symmetric to the sign of the buoyancy perturbations?

Answering these questions should help guide the interpretation of observations and the design of in interpretation of numerical experiments.

B.2   Model setup

We use VEROS (Häfner et al. (2018)), a purely Python based ocean model) with a setup similar to the idealized Atlantic slice setup of Munday et al. (2012) (see Fig. 3.1). The domain spans from $60°$ south to $60°$ north, and $30°$ in longitude. The depth is 4000 m, but with a sill of depth 2000 m located south of $40°$ S. The sill gives rise to periodic boundary conditions in the upper half of the southern part of the domain, and the setup is therefore a combination of both a basin and a (periodic) channel. This is to mimic the Atlantic basin together with Drakes' passage and the SO. The parameters used can be found in table B.1. The forcing applied to the model can be seen in Fig. 3.1: The upper surface is forced by a zonal wind stress given by

$$\tau_x(\theta) = \begin{cases} \rho \cdot 1.5 \cdot 10^{-4} \sin\left(\pi\frac{\theta+60°}{30°}\right), & \text{if } \theta < -30° \\ \rho \cdot -0.5 \cdot 10^{-4} \sin\left(\pi\frac{\theta-30°}{30°}\right), & \text{if } -30° < \theta < -5° \\ \rho \cdot -10^{-5}\left(1.5\cos\left(\pi\frac{\theta-10°}{10°}\right) + 2.5\right), & \text{if } -5° < \theta < 5° \\ \rho \cdot 0.5 \cdot 10^{-4} \sin\left(\pi\frac{\theta-30°}{30°}\right), & \text{if } 5° < \theta < 30° \\ \rho \cdot -5 \cdot 10^{-5} \sin\left(\pi\frac{\theta-60°}{30°}\right), & \text{if } 30° < \theta \end{cases} \tag{B.1}$$

The surface is relaxed to a temperature profile given by

$$T^*(\theta) = \begin{cases} T_s + \Delta T \sin\left(\pi\frac{\theta+60°}{120°}\right), & \text{if } \theta < 0° \\ T_n + (\Delta T + T_s - T_n)\sin\left(\pi\frac{\theta+60°}{120°}\right), & \text{if } 0° < \theta, \end{cases} \tag{B.2}$$

with $T_s = 0\,°\text{C}$, $T_n = 5\,°\text{C}$ and $\Delta T = 25\,°\text{C}$. The relaxation constant is found in table B.1. The north-south asymmetry with $5°\text{C}$ higher temperature in the North is to mimic

the temperature difference between the areas of deep convection in the North Atlantic and the southern most part of the SO.

Parameter	Symbol	Value	Units
Horizontal viscosity	ν_h	10^5	m^2/s
Time step	Δt	3600	s
Restoring timescale, salt	τ_S	30	days
Restoring timescale, temperature	τ_T	10	days
Horizontal resolution	-	2 degrees	°
Vertical resolution	10m (top) to	250m (bottom)	with 40 layers

Table B.1: Model parameters used in simulation

To address question 4, we set up a small ensemble of models with each of the three members having different κ. The chosen values of κ are $\kappa_{500} = 500 \, \text{m}^2/\text{s}$, $\kappa_{1000} = 1000 \, \text{m}^2/\text{s}$ and $\kappa_{2000} = 2000 \, \text{m}^2/\text{s}$. The models are spun up for 600 model years.

After this spin-up phase the circulation has four wind-driven cells (two in each hemisphere, see Fig. 3.2) and a current resembling the ACC flowing in the periodic channel. Also the circulation has a clear meridional overturning (MOC) with deep-water formation in the north and lift of deep water in the channel. The circulation also has a deep cell fed by water from the very south of the channel.

To be able to answer our questions we now change our forcing so that we generate 5 branches of our ensemble:

1. In the first branch - which members are called **-SALT*n***, where ***n = 500, 1000, 2000*** depending on κ - the salinity in the very north is relaxed towards a lower value. The relaxation profile is given by

$$S^*(\theta) = \begin{cases} S_n, & \text{if } -50° < \theta \\ S_n + \sin\left(\frac{-\pi}{2}\frac{50-\theta}{10°}\right), & \text{if } \theta < -50°. \end{cases} \tag{B.3}$$

   The relaxation constant is found in table B.1. This resembles the perturbation of Pedro et al. (2018).

2. In the second branch - members called **SALTEQ*n*** - the salinity is also relaxed as described by eq. B.3, and the winds over the equator are turned off:

$$\tau_x(\theta) = 0, \text{ for } -5° < \theta < 5°. \tag{B.4}$$

   This perturbation will help us address question 2

3. In the third branch - members called **SALTSO*n*** - the salinity is also relaxed, and the winds over the channel are moved slightly south:

$$\tau_x(\theta) = \begin{cases} \rho \cdot 1.5 \cdot 10^{-4} \sin\left(\pi\frac{\theta+60°}{28°}\right), & \text{if } \theta < -32° \\ \rho \cdot -0.5 \cdot 10^{-4} \sin\left(\pi\frac{\theta-30°}{30°}\right), & \text{if } -32° < \theta < -15° \end{cases} \tag{B.5}$$

This corresponds to moving the wind peak over the channel 1° south. This perturbation will help us address question 3.

4. The fourth branch has no salinity relaxation - called **OSO*n*** - and only the winds over the channel are moved slightly south as described by equation B.5. This will also help us to address question 3.

5. In a fifth branch - **+SALT*n*** - the salinity in the North is nudged towards a higher value (36 PSU), when going from 50° N to 60° N.

These 16 setups and the control are integrated for another 400 model years, and the output is compared to the control.

B.3 Results

First we consider the consequences of the perturbation applied to **-SALT*n***, which is a fresh water pertrubation at high northern latitude.

B.3.1 Collapse of the overturning

The strength of the overturning decreases significantly, when fresh water is released (See table B.2). We see that the decrease in the overturning is insensitive to our choice of κ, but that the initial and final strength of the overturning is sensitive to κ.

Kappa	Before leak	After leak	change
500	2.9 Sv	1.6 Sv	-1.3 Sv
1000	2.4 Sv	1.0 Sv	-1.4 Sv
2000	1.6 Sv	0.3 Sv	-1.3 Sv

Table B.2: Changes in the overturning defined as the maximum value of the overturning streamfunction (see Fig. 3.2) below 300 m depth at the equator .

By contrast, the circulation in the channel is independent on the value of κ and is insensitive to the fresh water perturbation (See table B.3).

Kappa	Before leak	After leak	Changes
500	3.5 Sv	3.3 Sv	-0.2 Sv
1000	3.6 Sv	3.5 Sv	-0.1 Sv
2000	3.7 Sv	3.7 Sv	0.0 Sv

Table B.3: Changes in Southern ocean circulation defined as the maximum value over the overturning stream function south of 40 ° S.

B.3.2   Propagation of temperature anomaly

To analyze the effect of the perturbation on the temperature distribution in the ocean, a temperature anomaly is calculated as the difference between the fresh water perturbed models and the control. For the branch **-SALTn** the temperature anomaly develops in qualitatively the same way for all values κ, and the initial phase shares a number of key features with the description by Kawase (1987): A negative salinity anomaly causes a warm anomaly that propagates as Kelvin wave to the equator along the western boundary. When it reaches the equator, it travels along the equator, and when the eastern boarder is reached, the wave splits up and propagates both north and south. The Kelvin wave radiates Rossby waves, that deepens the thermocline in the basin. This development is seen in Fig. 4.1. The temperature signal for all values of κ is strongest around 500 m depth. The overall result is a deepening of the thermocline in the ocean basin.

The time it takes for the signal to arrive in the channel is quite independent of κ (3-4 years, Fig. 4.5), and as soon as the channel is reached, the temperature starts to rise there.

Though a small temperature change can be noticed in the channel early, the rate of temperature change in the channel is significantly smaller than in the basin (Fig. 4.2). The changes to the zonally averaged temperature in the final state is comparable to the results Pedro et al. (2018) (2018, Fig. 4.3). Changes to equatorial winds have only a minor impact on this result (Fig 4.3), and the changes are confined to the upper part of the equatorial thermocline. Thus, we can conclude here that shifts of the ITCZ may be the result of AMOC changes, but they are not necessary to explain the South Atlantic warming as suggested by Pedro et al. (2018). The basic structure of the response is similar in the integrations with smaller and higher κ, except for the depth of the response. The depth of the thermocline is generally a function of thickness diffusion (see Ferreira et al. (2005)). Therefore the temperature response to the perturbation, which is a function of the stratification, is shallower as well (4.4).

The figure also highlights that the heat anomaly actually never completely crosses the ACC (as it is restricted to the outcropping of the thermocline isopycnals). However, as shown in Pedro et al. (2018) the warming of less than 1 degree leads to a melt of sea ice, which further heats the ocean due to the positive sea-ice/albedo feedback.

B.3.3   Warming Rates in the Southern Ocean

For all branches and ensemble members a time series of the average temperature change is calculated between 100 m and 700 m depth and $42°$ S to $51°$ S (Fig. 4.5).

We see that the change in temperature depends on κ, so that lower κ, means higher temperature increase. As we have seen already there is a small dependency on whether or not we change the winds over the channel. This is most easily seen with the dotted lines, which show that a change in the position of the SO winds has only little impact on the SO

temperature. Similarly, the change in wind over the equator does not induce any change in the channel at all.

Fig. 4.5 shows that the time it takes for the signal to arrive in the channel is quite independent of κ (3-4 years). This is no surprise since the signal arrives in the channel by means of wave transport and not eddy diffusion.

As soon as the wave has reached the channel, a temperature increase can be noticed all across the channel. The temperature increase saturates over time, and 30% of the final temperature change is reached after approximately 30 years for all values of κ (fig 4.5). This value is consistent with a simple scaling of diffusive time scales, $O(T) = O(L^2/\kappa)$, which for a length scale of 1000 km and a κ of 1000 m^2/s also yields 30 years. The detailed value of κ has only little impact, because the temperature flux of parameterized eddies does not only depend on the diffusion coefficient and the temperature gradient, but also on the slope of the isopycnals (Griffies (2003)). As we see from Fig. 4.4 the high κ also have the weakest slope of the temperature anomaly field and the density field. This decreases the response time.

B.3.4 Asymmetry of positive and negative salinity perturbations

The basic arguments of Kawase (1987) and Schmittner et al. (2003) are independent of the sign of the perturbations. Also, Pedro et al. (2018) suggest that the response is mostly linear. The ocean, however, is nonlinear, and it is important to check if these nonlinearities affect our results. Most simply this is done by reversing the sign of the perturbations.

Comparing Fig. 4.4 and Fig. 4.5 to Fig. 4.6, one finds that to the lowest order there is little difference apart from the sign. However, the anomalies do reach deeper and further south. This is because a positive salinity perturbation strengthens the overturning and affects isopycnals that outcrop closer to the southern boundary (fig 4.7).

The response is otherwise similar to **-SALT*n***: The magnitude of the anomaly is independent of κ for **+SALT*n*** (0.47 - 0.53 $^\circ C$) but larger then for **-SALT*n*** (0.22 - 0.36 $^\circ C$). The response time too is similar, approximately 30 years to reach one third of the final state. Again we see that the size of the diffusivity, κ and the isopycnal slope balance out each other, so that we get a response time that is independent of κ - and also independent of the sign of the perturbation.

B.4 Summary and Discussion

A negative salinity perturbation is applied at high northern latitude in an idealised Atlantic sector ocean model. The model consists of a basin and a channel, and is forced by a temperature relaxation profile and a constant wind profile (see Fig. 3.1). The salinity perturbation gives rise to a southward traveling temperature signal: A warm signal, when

the perturbation is fresh. A cold signal, when the perturbation is salt. The propagation can be decomposed into two parts: A fast part in the basin that consists of Kelvin and Rossby waves, and a slow temperature diffusion across the channel.

- We find that travel time of the signal, and magnitude of the response is independent of wind changes near the equator or over the channel.

- Both the wave travel time ($\sim$4 years) in the basin and the eddy response time ($\sim$30 years) in the channel are similar for all values κ. In contrast the magnitude of the temperature change does depend on κ, with a low κ giving the largest response.

- For a positive salinity perturbation, the magnitude of the temperature change is approximately 50% larger than for a negative perturbation, but the response time is the same.

These results provide support for one of the interpretation of the results by Pedro et al. (2018): a purely oceanic pathway exist that connects the North Atlantic to the Southern Ocean. Our results also provide support for the Schmittner et al. (2003) hypothesis that the minimum timescale of this connection is determined by turbulent diffusion across the ACC. For future modelling studies it is comforting to know that the timescale and strength of this connection is robust to different surface forcings or strengths of turbulent diffusion.

Published results from the analysis of ice cores find a 200 year timelag between the onset of a stadial and the onset of Antarctic warming (WAIS Divide Project Members (2015)), arguably with some uncertainty (Buizert et al. (2018)). Results of coupled models also find 200 years (Pedro et al. (2018), Nielsen et al. (2019)). If the ocean alone would set the timescale of the response, our results suggest that the lag between Antarctic warming and the onset of a stadial should be less than 100 years (Fig. 4.5). However, while Pedro et al. (2018) showed unambiguously that the Southern Ocean warming is indeed started by increased heat fluxes across the ACC, they also pointed out that a further necessary process in the chain of events is the melting of sea-ice around Antarctica. Thus, based on the present results we conclude that the time scale of the bipolar seasaw is not determined by ocean dynamics, but rather by the thermal inertia of the Southern Ocean mixed layer and its sea-ice cover.

B.4.1 Acknowledgements

B.5 Figure captions

Figure 3.1: *The model consists of a basin that spans from* $40°$ *S to* $60°$ *N, and a channel in the southern part. The channel has a sill to resemble the Drakes passage. The wind stress profile is shown in blue, and the temperature relaxation is shown in red*

Figure 3.2: *Barotropic and residual meridional streamfunction (RMS) for the spun-up model for* κ_{500}. *The RMS shows a hemisphere crossing overturning cells in both the upper (fed by deep water from the north) and lower (fed with water from most southern part of the channel) part of the basin. The barotropic streamfunction shows wind-driven cells and and a zonal current in the periodic channel*

Figure 4.1: *Temperature anomaly for **-SALT500** in 500 m. The equator and boundaries first heat up due to kelvin waves. The interior warms due to Rossby waves.*

Figure 4.2: *Hovmöller diagram for the zonally averaged temperature at 500 m depth for **-SALT500**. A wave signal is seen the first 5 years. After this a slower diffusive signal is seen in the channel (*$40°$ *to* $60°$ *S).*

Figure 4.3: *Zonal average of the temperature anomaly after 400 years. The upper figure shows **-SALT500**. The lower figure **SALTEQ500**. We see that these two only differ in the surface layer right at the equator. In the southern hemisphere, the temperature anomaly follows isopycnals almost all the way to the outcrop point, where the anomalies bend northward.*

Figure 4.4: *-SALTn, and for **SALTOS2000**. The signal is always arrested by isopycnals. A southward shift of the wind doesn't change the location of the anomaly or the structure of the isopycnals.*

Figure 4.5: *The upper figure shows the temperature anomaly from 100 m to 700 m depth between 42* ° *S and 51* ° *S for* κ_{500}, κ_{1000} *and* κ_{2000}. *The solid lines show **-SALTn** the* $-\cdot-$ *dashed lines are **SALTOSn**, and the* $\cdots$ *dashed lines show **OSOn**. The figure also shows **SALTEQn**, but these lines coincide with those of **-SALTn**, and are therefore hard to see. The lower figure shows the initial phase of the warming with normalized values (divided by their maximum value) for **-SALTn**.*

Figure 4.6: *The figure shows the temperature anomaly after 400 years for **+SALTn**. The lower left figure shows a time series of the temperature anomaly in the northern half of the channel. Just like for **-SALTn** the response time for the temperature change in the channel is independent of* κ, *but unlike **-SALTn**, the magnitude of the response is also*

*independent. In contrast to **-SALTn**a higher κ means a further southward propagation of the temperature anomaly. There is a tendency for the anomaly to cross isopycnals.*

Figure 4.7: *Salinity anomaly profile 400 years after the perturbations are applied. The upper part shows **-SALTn** and the lower part shows **+SALTn**. We see that salinity changes propagate further south **+SALTn**. This means that for **-SALTn** both temperature and salinity are dynamical tracers in the Channel.*